

# Observational Signature of Tidal Disruption of a Star by a Massive Black Hole

T. Bogdanović, M. Eracleous, S. Sigurdsson, P. Laguna  
*Pennsylvania State University, PA 16802, USA*  
 S. Mahadevan  
*University of Florida, FL 32611, USA*

We have modeled the time-variable profiles of the H $\alpha$  emission from the nonaxisymmetric disk and debris tail created in the tidal disruption of a solar-type star by a  $10^6 M_\odot$  black hole. Two tidal disruption events were simulated using a three dimensional relativistic smoothed particle hydrodynamic code to describe the early evolution of the debris during the first 50-90 days. We have calculated the physical conditions and radiative processes in the debris using the photoionization code CLOUDY. We model the emission-line profiles in the period immediately after the accretion rate onto the black hole becomes significant. We find that the line profiles at these very early stages of the evolution of the postdisruption debris do not resemble the double-peaked profiles expected from a rotating disk, since the debris has not yet settled into such a stable structure. As a result of the uneven distribution of the debris and the existence of a “tidal tail” (the stream of returning debris), the line profiles depend sensitively on the orientation of the tail relative to the line of sight. Moreover, the predicted line profiles vary on fairly short time scales (of order hours to days). Given the accretion rate onto the black hole we also model the H $\alpha$  light curve from the debris.

## 1. INTRODUCTION

A star in an orbit around a massive black hole can get tidally disrupted during its close passage by the black hole. After several orbital periods the debris from the disrupted star settles into an accretion disk and gradually falls into the black hole [1, 2, 3, 4]. As material gets swallowed by the black hole intense UV or soft-X ray radiation is expected to emerge from the innermost rings of the accretion disk [5, 6, 7, 8, 9, 10, 11, 12]. For black hole masses  $M_{bh} < 10^7 M_\odot$ , tidal disruption theory predicts flares with luminosities of the order of the Eddington luminosity with durations of the order of months, and with spectra that peak in the UV/X-ray band [1, 13, 14, 15, 16]. High-energy flares from the central source illuminate the debris, the photons get absorbed, and some are re-emitted in the optical part of the spectrum (i.e. the light is “reprocessed”). One of the spectral lines in which this phenomenon can be observed is the Balmer series H $\alpha$  line ( $\lambda_{rest} = 6563 \text{ \AA}$ ).

The disruption of a star begins when the star approaches the tidal radius,  $r_t \simeq r_\star (M_{bh}/M_\star)^{1/3}$ , the point where the surface gravity of the star equals the tidal acceleration from the black hole across the diameter of the star ( $r_\star$  and  $M_\star$  are the radius and mass of the star and  $M_{bh}$  is the mass of the black hole). A  $10^6 M_\odot$  black hole is often used as a prototypical example in tidal disruption calculations. This choice is motivated by the criterion for a solar-type star to be disrupted before it crosses the black hole event horizon (i.e. the Schwarzschild radius,  $r_s$ ) in order for emission to be observable. For supermassive black holes with  $M_{bh} > 10^8 M_\odot$ ,  $r_s > r_t$  and the star falls into the black hole before it gets disrupted.

## 2. CALCULATION

Tidal disruption simulations were carried out with a three dimensional relativistic smoothed particle hydrodynamics (hereafter SPH) code in order to study the dynamical evolution of the post-disruption debris. The SPH code used provides a description of relativistic fluid flows in a static curved spacetime geometry [17, 18]. We use it to simulate the tidal disruption of a star in the potential of a Schwarzschild black hole.

Two different simulations were carried out with 5,000 and 20,000 particles (hereafter 5k and 20k respectively) contributing equally to the mass of a  $1 M_\odot$  star. The 5k calculation follows the debris for 94 days in total. After 34 days, significant accretion onto the black hole begins. Our investigation follows the evolution of the line profiles in the last 60 days. The 20k simulation spans 53 days, during which the evolution of the line profiles was followed for the last 6 days. Using both the 5k and 20k simulations in the line profile modeling we take advantage of the longer time span in the former and better resolution achieved with the larger number of particles in the latter. Figure 1 shows particle distribution maps after the second pericentric passage, at the beginning of the accretion phase and at the end of the 5k simulation. At the early stages of the tidal event most of the particles were located in the pronounced *tidal tail*. Sixty days later, about 20% of the particles are scattered from the tidal tail and form a quasi-spherical distribution, with most of its mass concentrated in the equatorial plane. We refer to the spheroidal part of the debris as the *halo* and to its planar component as the *disk*. There is a concern that some fraction of particles of the halo are a numerical artifact of the simulation. We further mention the implications of existence of the spheroidal halo for

the total H $\alpha$  luminosity and emission line profiles in §3.1 and §3.2.

We follow the line profile calculations carried out by [19] and [20] to obtain the observed profile from a Keplerian, relativistic, thin disk in the weak field approximation. The main objective of the calculation is to obtain the final expression for the flux density in the observer's frame as a function of parameters defined in the reference frame of the debris.

In order to calculate the resulting H $\alpha$  luminosity of the debris it is necessary to determine the efficiency with which the debris reprocesses the incident radiation. This efficiency can be characterized by the surface emissivity of the debris as a function of radius,  $\epsilon = \epsilon_0 \xi^{-q}$ , where  $\epsilon_0$  is a constant and  $\xi \equiv r/r_g$  is the dimensionless radius ( $r_g = r_s/2 = GM_{bh}/c^2 = M_{bh}$ ). We have used the photoionization code CLOUDY [21] for numerical calculations of the response of the debris to illumination. For a more detailed description of the calculation refer to [22].

### 3. RESULTS

#### 3.1. Light Curves

With the above emissivity prescriptions we have calculated the *observed* H $\alpha$  luminosity curve of the debris at a particular time step by computing the time at which the light was emitted from the debris and by finding the ionizing flux that was illuminating that location at the time the emission occurred, according to the light-travel time from the black hole to that particular region of the debris. We assumed that the observer is located in the x'z' plane, above the orbital plane at  $i = 30^\circ$  to the z'-axis, at a distance  $d \rightarrow +\infty$ .

Figure 2 shows three different H $\alpha$  light curves from the debris confined to a plane (assuming  $\xi_{in} = 500$ ,  $\xi_{out} = 40,000$ ) during the 60-day accretion phase of the 5k simulation. Figure 2a shows the accretion luminosity on a logarithmic scale (solid curve), calculated from the accretion rate of the debris in the simulation. The UV/X-ray luminosity curve is arbitrarily scaled and overplotted on the top of the H $\alpha$  curve for comparison. The H $\alpha$  light curve departs from the accretion light curve at late times, though the departure appears small in the logarithmic plot (used here due to the large dynamic range of the light curves). The same effect is more noticeable in Figure 2b, where the accretion luminosity is proportional to  $t^{-5/3}$  and the H $\alpha$  light curve is plotted on a linear scale. The H $\alpha$  light curve roughly follows the shape of the incident UV/X-ray light curve at early times but decays faster at late times. The faster decay in the H $\alpha$  light curve reflects the debris evolution in time: as the tail becomes more elongated, the incident photons travel a longer way to illuminate the debris. Consequently, the intensity of the illuminating light gets lower in

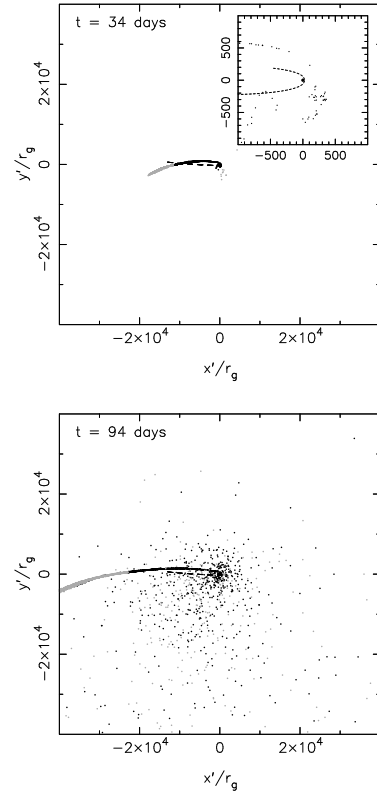


Figure 1: Maps showing the positions of the SPH particles from the 5k simulation after the second pericentric passage, projected in the x'y'-plane at two different times. Particles gravitationally bound to the black hole are colored black, while unbound particles are colored grey. The dashed line represents the initial trajectory of the star before disruption and the trajectory of the center of mass of the debris after disruption. The maximum particle velocities are of order  $10^{-2}c$ . *Upper Panel:* Particle map at the start of the accretion phase, 34 days after the disruption occurred. Inset: Particles in the inner region of the debris, orbiting close to the black hole. *Lower Panel:* Particle map at the end of the simulation, 94 days after the disruption. The tidal tail can be clearly separated into particles that are unbound and about to escape the black hole and particles that are returning towards the black hole. The inner region of the debris consists of returning particles from the inner tail that have been scattered and form a flat rotating structure around the black hole.

the later stages of the tidal disruption event. At late times the decay of H $\alpha$  light curve stops because of the return of more particles from the tail to the immediate vicinity of the black hole. As particles diffuse from the high density tail to the lower density disk, in later stages of the simulation, their emission efficiency increases and they contribute a significant amount of H $\alpha$  light to the light curve. To isolate the effect of the

debris evolution in time from the evolution of the illuminating light curve, we calculate the H $\alpha$  light curve in the case of constant illumination (Fig. 2c). Here, the relative departure of the H $\alpha$  light curve from the UV/X-ray light curve can be interpreted as a consequence of the expansion and redistribution of the debris. The H $\alpha$  luminosity appears to level off at late times because the debris disk begins to settle into a quasi-steady configuration.

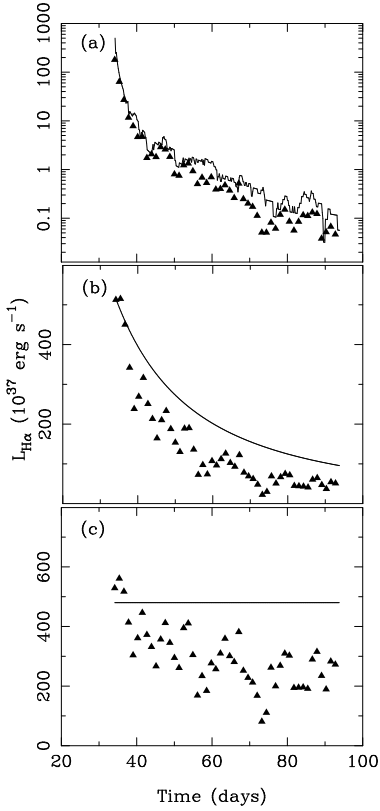


Figure 2: The H $\alpha$  light curves (triangles) resulting from the reprocessing of three different illumination light curves. The solid line shows a scaled version of the UV/X-ray continuum light curve that illuminates the debris, which in (a) follows the SPH accretion rate, (b) decays with time as  $t^{-5/3}$ , and (c) is constant. Note that the vertical axis is calibrated logarithmically in (a), while in (b) and (c) they have the same linear scale. The H $\alpha$  light curves rise initially as the illumination front propagates through the debris and then decay faster than the UV/X-ray light curves.

The observed H $\alpha$  flux depends sensitively on the UV/X-ray light curve, on the distribution of matter that makes up the inner portion of the debris, and on how quickly particles redistribute themselves in phase space. The main features of the H $\alpha$  light curve are: an initial rise followed by a decline, with superposed fluctuations. The initial rise is a consequence of the propagation of the initial illumination front through the debris. The fluctuations are a result of the fluc-

tuations in the accretion rate, which are caused, in turn, by the finite number of particles employed in the simulation. The decay rate of the H $\alpha$  light curve is determined by the decay rate of the UV/X-ray light curve, debris expansion and redistribution rate.

The CLOUDY calculation predicts a time-average H $\alpha$  luminosity from the tidal debris of about  $10^{36}$ ,  $10^{37}$ , and  $6 \times 10^{38}$  erg s $^{-1}$  for the tail, disk and halo, respectively. In the earlier stages of the disruption event when the UV/X-ray luminosity is super-Eddington, the H $\alpha$  luminosity is expected to be up to 80 times higher than its average value and comparable to that of tidal disruption candidates observed in the local universe (see Figure 2). These examples include NGC 4450 (at 16.8 Mpc) with an H $\alpha$  luminosity of  $L_{H\alpha}=1.8 \times 10^{39}$  erg s $^{-1}$  [23] and NGC 1097 (at 22 Mpc) with  $L_{H\alpha}=7.7 \times 10^{39}$  erg s $^{-1}$  [24]. Thus the emission-line signature of a tidal disruption event should be detectable at least out to the distance of the Virgo cluster. In practice, however, the detection of such emission lines from low luminosity sources may be complicated by their weak contrast relative to the underlying stellar continuum.

### 3.2. Line Profiles from the Debris

In Figures 3–6 we show sample line profiles to illustrate how they evolve in time and how they are affected by the choice of model parameters and by the orientation of the observer. Figure 3 is a “trailed spectrogram” summarizing the temporal evolution of the line profiles from the two different SPH runs; it is a 2-dimensional map of the H $\alpha$  emission as a function of projected velocity and time. Figure 4 shows a different representation of the evolution of the line profile with time, which effectively comprises selected time slices from the trailed spectrogram. Figures 5 and 6 show how the inner radius of the line-emitting region and the azimuthal orientation of the observer affect the observed line profiles.

A property that is immediately obvious in the line sequence is the change of the profile shape with time

(Figures 3 and 4). The adopted low value of velocity dispersion allows us to resolve individual particles in the trailed spectrograms, orbiting around the black hole. The evolution of the line intensities in time roughly follows the behavior of the UV/X-ray luminosity but decays somewhat faster in time. The multi-peaked line profile is a consequence of the velocity field of the inner debris, which consists of the inner portion of the tidal tail that is falling towards the black hole (towards the observer) and debris that is rotating around the black hole after being scattered. The line profiles and their variability could be observationally important features of the debris just formed from tidal disruption. The variable line profiles might be observed and recognized on the relatively short

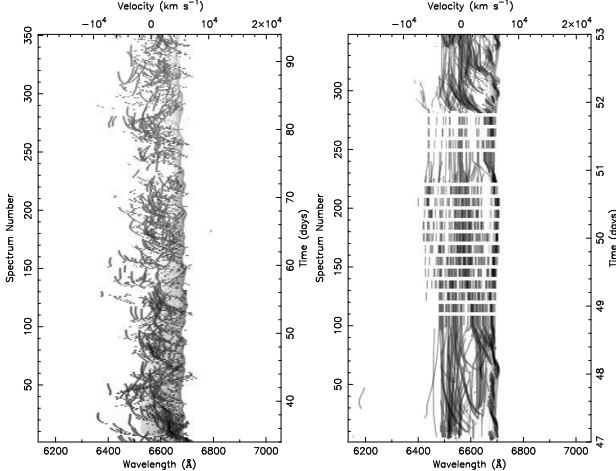


Figure 3: Trailed spectrogram of the simulated H $\alpha$  emission-line profiles from the 5k simulation spanning 60 days (left) and from the 20k simulation spanning 6 days (right). This is effectively a 2-dimensional intensity map versus projected velocity of the emitting material and time. Darker shades correspond to higher intensity. The scale on the right represents time since the tidal disruption event.

time scale of hours to days.

The profiles become broader as the inner radius of the line-emitting regions decreases since higher-velocity gas resides at smaller radii (see Figure 5). The approximate full width at zero intensity of the profiles ranges from 4,500 km s $^{-1}$  for  $\xi_{in} = 10,000$  to 18,000 km s $^{-1}$  for  $\xi_{in} = 200$ . We find that line profiles change from the profiles dominated by the emission red-ward from the rest wavelength for  $\xi_{in} < 1000$  to narrower profiles dominated by the blue-ward emission from the tail for  $\xi_{in} > 1000$ , since for large values of  $\xi_{in}$ , the high-velocity rotating gas in the vicinity of the black hole is excluded and the dominant contributions to the line profile come from the tidal tail. The intensity of the line also decreases with increasing inner radius, making the outer regions of the debris harder to observe.

Because of the non-axisymmetric geometry and velocity field, the line profiles emitted by the debris, depend on the orientation of the tidal tail relative to the observer. In Figure 6 we show the effect of azimuthal orientation  $\phi_0$  of the debris, with respect to the observer. The values of  $\phi_0$  are 45°, 90°, 120°, 180°, 220° and 270°, as measured in a counterclockwise direction from positive x'-axis to the observer's line of sight. These can be compared with the profile corresponding to the same time in Figure 4 for  $\phi_0 = 0^\circ$ . The position of the peaks in Figure 6 varies relative to the rest wavelength, since the relative direction of bulk motion of the material depends on the observer's orientation. For example, it is possible to distinguish

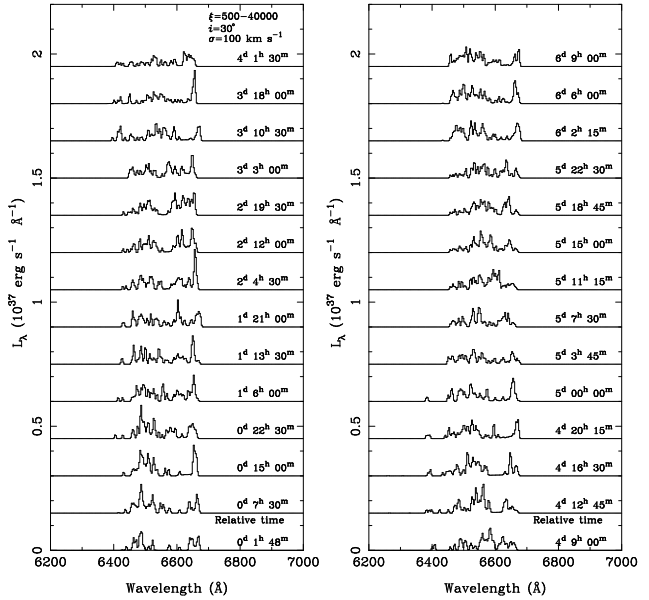


Figure 4: Sequence of H $\alpha$  profiles emitted from the region  $\xi \in (500, 40,000)$  over a period of 6 days (20k run). The relative time from the beginning of the accretion phase onto the black hole is marked next to each profile. The accretion phase begins 47 days after the tidal disruption. The inclination of the debris plane and the velocity shear are as marked on the figure.

the emission from the tail for the range of azimuthal orientations 90° – 220°. The tail emission in these profiles appears as the most blueshifted peak, since these are the orientations for which different portions of the tail flow towards the observer.

We have computed model profiles for several different X-ray illumination light curves keeping all the other parameters fixed. We used (a) the light curve obtained from the accretion rate in the 5k simulation, (b) the light curve from the accretion rate as predicted by theory, i.e.  $\propto t^{-5/3}$  [1, 8], and (c) a light curve that is constant in time (Figure 2). We find that the line profile shapes do not depend sensitively on the shape of the light curve. This is a consequence of the centrally "weighted" emissivity profile of the debris which causes the innermost emission region to be the dominant contributor of the H $\alpha$  light. In the innermost region of the debris the dynamic range in light-travel times is not large; therefore the illumination of the innermost emitting region is almost instantaneous. Over the very short light-crossing time of the central emitting region, the gradient in the UV/X-ray light curve is small and the illumination is nearly constant over this region. The fast fluctuations in the illuminating light curve on the other hand are smoothed out during reprocessing in the debris, and cannot be identified in the H $\alpha$  light curve.

The temporal variability of the H $\alpha$  emission line profiles from the post-disruption debris is one of the

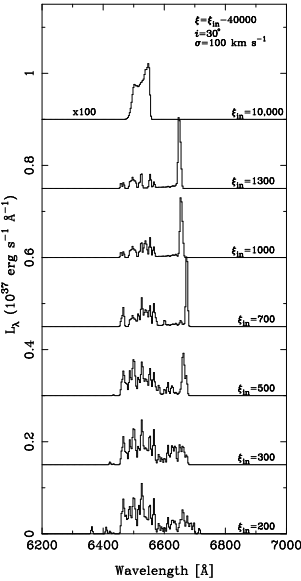


Figure 5: H $\alpha$  emission line profiles simulated for seven different values of inner radius ( $\xi_{in}$ ), as determined by the propagation of the ionization front through the debris. The relative time for profile frames is  $6^d 6^h 0^m$ . The intensity of the profile calculated for  $\xi_{in} = 10,000$  is multiplied by the factor of 100. The inclination and velocity shear are as marked on the top of the figure.

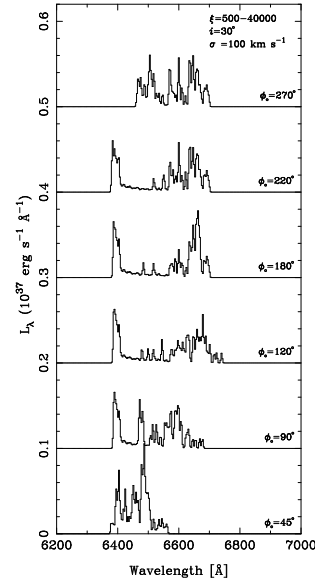


Figure 6: H $\alpha$  emission line profiles simulated for six different azimuthal orientations of the debris with respect to the observer, as represented by  $\phi_0$ . See profile in Figure 4 with the time label  $5^d 22^h 30^m$  for orientation  $\phi_0 = 0^\circ$ . The size of the emitting region, inclination and velocity shear are as marked on the top of the figure.

## 4. CONCLUSIONS

We modeled the emission-line luminosity and profile from the debris released by the tidal disruption of a star by a black hole in the early phase of evolution. Our model predicts prompt optical evolution of the post-disruption debris and profile shapes different from circular and elliptical disk model profiles. Since line profiles observed so far in LINERs (low-ionization nuclear emission regions) look more disk-like and evolve slowly, the observations are likely to have caught the event at late times ( $\geq 6$  months after the initial disruption), after the debris has settled into a quasi-stable configuration.

The line profiles can take a variety of shapes for different orientations of the debris tail relative to the observer. Due to the very diverse morphology of the debris, it is almost impossible to uniquely match the multi-peaked profile with the exact emission geometry. Nevertheless, the profile widths and shifts are strongly indicative of the velocity distribution and the location of matter emitting the bulk of the H $\alpha$  light. Profile shapes do not depend sensitively on the shape of the light curve of the X-rays illuminating the debris. They strongly depend on the distance of the emitting material from the central ionizing source, which is a consequence of the finite propagation time of the ionization front and the redistribution of the debris in phase space. It may be possible to distinguish between the two effects observationally, based on their different characteristic time scales.

important indicators of a tidal disruption event. In order to capture the rapid profile variability, due to the variable illumination, the exposure time should be comparable to the light crossing time of the innermost regions of the line-emitting debris, which has the fastest and strongest response to the ionizing radiation. Longer exposures are expected to capture the average shape of the rapidly varying line profiles. The light-crossing time of the innermost regions of the debris is about  $8 \xi_2 M_6$  minutes (where  $\xi_2 = \xi/100$  and  $M_6 = M_{bh}/10^6 M_\odot$ ), while the exposure times are typically about 30-60 minutes (for galaxies at the distance of the Virgo cluster, for example). Thus, if an event is caught early in its evolution and the light-crossing time is relatively long (i.e.,  $M \gtrsim 10^6 M_\odot$ ), there is a chance of detecting variability caused by changing illumination over the course of one to a few nights. On longer time scales, variability is caused by changes in the structure of the debris. In the presence of the spheroidal halo, the variability of the lines may be modified by the long diffusion time scale of photons through the halo. The component of the tidal tail outside the halo will then still respond to the variability but on the time scale set by the light reprocessed by the halo.

If X-ray flares and the predicted variable profiles could be observed from the same object they could be used to identify the tidal disruption event in its early phase. The X-ray flares can be promptly detected by all-sky synoptic X-ray surveys and high energy burst alert missions such as *Swift*. The evolution of the tidal event may then be followed with optical telescopes from the ground on longer time scales and give an insight in the next stage of development of the debris. Thus, simulations of the tidal disruption process on longer time scales (of order several months to a few years) are sorely needed. Calculations of the long-term evolution of a tidal disruption event can predict the type of structure that the debris finally settles into and whether its emission-line signature resembles the transient double-peaked lines observed in LINERs. This study would provide an important insight into the evolution of LINERs.

Finally, the observed rate of tidally disrupted solar type stars can constrain the rate of captured compact objects which are important gravitational wave sources [25, 26, 27], and the capture rate of main sequence stars in our Galaxy, which are expected to emit the peak of the gravitational radiation in the LISA frequency band and can be detected in the local universe [28].

## Acknowledgments

We acknowledge the support of the Center for Gravitational Wave Physics which is funded by the National Science Foundation under cooperative agreement PHY 01-14375, NSF grants PHY 98-00973 and PHY 02-44788, the Zaccheus Daniel Fellowship, and the Eberly College of Science.

## References

- [1] Rees, M. 1988, *Nature*, 231, 91
- [2] Cannizzo, J. K. Lee, H. M., & Goodman, J. 1990, *ApJ*, 351, 38
- [3] Syer, D. & Clarke, C. J. 1992, *MNRAS*, 255, 92
- [4] Loeb, A., & Ulmer, A. 1997, *ApJ*, 489, 573
- [5] Frank, J. & Rees, M. J. 1976, *MNRAS*, 176, 633
- [6] Lightman, A. P. & Shapiro, S. L. 1977, *ApJ*, 211, 244
- [7] Frank, J. 1978, *MNRAS*, 184, 87
- [8] Phinney, E.S. 1989 in IAU Symp. 136, The Center of the Galaxy, ed. M.Morris (Dordrecht: Kluwer), 543
- [9] Sembay, S. & West, R. G. 1993, *MNRAS*, 262, 141
- [10] Magorrian, J. & Tremaine, S. 1999, *MNRAS*, 309, 447
- [11] Syer, D. & Ulmer, A. 1999, *MNRAS*, 306, 35
- [12] Donley, J. L., Brandt, W. N., Eracleous, M., & Boller, T. 2002, *AJ*, 124, 1308
- [13] Evans, C. R. & Kochanek, C. S. 1989, *ApJ*, 346, L13
- [14] Ulmer, A. 1999, *ApJ*, 514, 180
- [15] Kim, S. S., Park, M.-G., & Lee, H. M. 1999, *ApJ*, 519, 647
- [16] Gezari, S., Ghez, A. M., Becklin, E. E., Larkin, J., McLean, I. S., & Morris, M. 2002, *ApJ*, 576, 790
- [17] Laguna, P., Miller, W. A. & Zurek, W. H. 1993a, *ApJ*, 404, 678
- [18] Laguna, P., Miller, W. A., Zurek, W. H., & Davies, M. B. 1993, *ApJ*, 410, L83
- [19] Chen, K. & Halpern, J.P. 1989, *ApJ*, 344, 115
- [20] Eracleous, M., Livio, M., Halpern, J.P. & Storchi-Bergmann, T. 1995, *ApJ*, 438, 610
- [21] Ferland, G. J. 1996, Hazy, a Brief Introduction to CLOUDY (Lexington: Univ. Kentucky, Dept. Phys. Astron.)
- [22] Bogdanović, T., Eracleous, M., Mahadevan, S., Sigurdsson, S., & Laguna, P. 2004, *ApJ*, 610, 707
- [23] Ho, L. C., Rudnick, G., Rix, H., Shields, J. C., McIntosh, D. H., Filippenko, A. V., Sargent, W. L. W., & Eracleous, M. 2000, *ApJ*, 541, 120
- [24] Storchi-Bergmann, T., Eracleous, M., Livio, M., Wilson, A. S., Filippenko, A. V., & Halpern, J. P. 1995, *ApJ*, 443, 617
- [25] Sigurdsson, S. & Rees, M. J. 1997, *MNRAS*, 284, 318
- [26] Hils, D & Bender, P. L. 1997, *ApJ*, 445, L7
- [27] Freitag, M. 2001, *Class. Quant. Grav.*, 18, 4033
- [28] Freitag, M. 2003, *ApJL*, 583, L21